The XMGUN Particle Path FEM Code

César C. Xavier[1] and Cláudio C. Motta[2]

[1]Instituto de Pesquisas Energéticas e Nucleares/CNEN-SP, São Paulo 05508, Brazil
[2]Universidade de São Paulo, São Paulo 05508-000, Brazil

This work reports some initial results of a 2-D electron gun design code (XMGUN) based on the finite-element method (FEM). Using the Galerkin weak formulation, the nodal analysis, and the first-order elements, the Poisson equation was solved for the electron gun electrostatic potential. The nonrelativistic particle paths were numerically calculated by a fourth-order Runge–Kutta method. An iterative scheme was repeated until the electron paths convergence was achieved under full space-charge limited condition. In order to validate the algorithm, the focusing properties of a 2-D Pierce electron gun with planar symmetry were studied. The quality of the beam was evaluated based on the particle's final position, the transit time, and the particle energy evaluations. Using these three parameters, a good agreement was found between the theoretical and calculated results. Absolute current density errors of less than 1% were found, even with a coarse discretization of the domain. The XMGUN tool was used to design a 30-kV, 7.1-A, and 1.37-μPerv axis-symmetric high-power electron gun for use in vacuum microwave devices. The figure of merit used as reference to measure the quality of the electron beam was the normalized transverse velocity.

***Index Terms*—Electron gun, electron path, finite-element method (FEM).**

I. Introduction

THE focusing properties of the electron guns, used in power microwave tubes design, can be investigated by analyzing the charged particle path. Knowledge about the particle paths in an electron gun is relevant, since these paths establish the beam edge, the beam waist, and the beam waist distance from the cathode. However, to the authors' knowledge, the existing gun codes, such as [1]–[5], use motion equation instead of the path equation. This work proposes a new methodology to solve the self-consistent space-charge limited condition from the particle path. Based on this approach, the newly developed tool was used to design a 30-kV, 7.1-A, and 1.37-μPerv, axis-symmetric high-power electron gun for use in vacuum microwave devices. The normalized transverse velocity was used as a figure of merit in measuring the quality of the electron beam.

The work is organized as follows. Section II presents the physical formulation of the problem, the finite element method (FEM), the derivation of the second-order differential equation for the nonrelativistic charged-particle path, and the self-consistent algorithm. Section III shows the code's benchmark consisting in a Pierce planar diode, and the most relevant results are discussed. Finally, the conclusions follow in Section IV.

II. Theoretical Description of the Problem

A. Physical Formulation

In order to obtain the scalar potential, a code using FEM with first-order triangle elements was developed. The planar symmetric electron steady-state flow can be described by the Poisson equation for the scalar potential in orthogonal curvilinear coordinates $\psi(u,v)$ as

$$\nabla^2\psi = \frac{1}{h_u h_v}\left[\frac{\partial}{\partial u}\left(\frac{h_v}{h_u}\frac{\partial\psi}{\partial u}\right)+\frac{\partial}{\partial v}\left(\frac{h_u}{hv}\frac{\partial\psi}{\partial v}\right)\right] = -\frac{1}{\varepsilon_0}\sum_i q_i\delta(u-u_i)\delta(v-v_i) \quad (1)$$

where the right-hand side refers to the space charge. q_i represents the ith charge of the macroparticle that is transported by the beam current of the electron gun located at the position (u_i, v_i). $\delta(u-u_i)$ and $\delta(v-v_i)$ denote the Dirac delta functions. The scale factors h_u and h_v, in rectangular coordinates, are equal to 1. In cylindrical coordinates, due to the transformation $x=\rho\cos\phi, y=\rho\sin\phi$ and $z=z, h_u=h_\rho=1$ and $h_v=h_\phi=1$ hold.

The charged-particle path is determined using the Lorentz force under the condition $(v/c)^2 \ll 1$ and the energy conservation law

$$\frac{d^2u_i}{dv_i^2} = \frac{1}{2\psi_i}\left[1+\left(\frac{du_i}{dv_i}\right)^2\right]\left(-E_{u_i}+E_{v_i}\frac{du_i}{dv_i}\right) \quad (2)$$

where the subscript i represents the ith particle path of the problem and $\overrightarrow{E} = -\nabla\psi$ is the electric field. Equation (2) shows that the particle path does not depend on the particle charge and mass ratio.

To solve the coupled problem (1)–(2), an in-house FEM code was used to determine the scalar potential and therefore the electric field. Then, to find the solution of (2), the second-order differential equation is transformed into a two first-order differential equation system, and then an in-house fourth-order Runge–Kutta integrator, with constant step size, is used. It is worth noting that the particle path slope can be directly extracted from the Runge–Kutta integration output. This leads to, for each particle path, a fast evaluation of the minimum of the path, which would be used to establish the beam waist and hence the beam waist distance from the cathode.

Since it is necessary to satisfy the charge conservation law, the total current I inside the device is constant.

Manuscript received December 22, 2009; revised February 24, 2010; accepted February 28, 2010. Current version published July 21, 2010. Corresponding author: C. C. Xavier (e-mail: cesarcx@usp.br).

Color versions of one or more of the figures in this paper are available online at http://ieeexplore.ieee.org.

Digital Object Identifier 10.1109/TMAG.2010.2045226

B. Finite Element Formulation

Due to accuracy and versatility of weighted residual methods, such as the Galerkin method, the FEM [6], [7] has been adopted as a standard for solving electromagnetic problems. The triangular finite element scalar potential V_e is written as $V_e(u,v) = \sum \Phi_i V_i$, where V_1, V_2, and V_3, respectively, are the unknown potential at nodes 1, 2, and 3, respectively, and $\Phi_i = \Phi_i(u,v)$ represents the basis functions. This leads to the following system of equations:

$$[S][U] + [g] = 0 \tag{3}$$

where

$$S_{ij} = \int_{\Omega} \nabla\Phi_i \cdot \nabla\Phi_j d\Omega \tag{4}$$

$$U_i = V_i \tag{5}$$

and

$$g_i = \frac{1}{\varepsilon_0} \int_{\Omega} \Phi_i \rho_i d\Omega \tag{6}$$

where ρ_i is the right-hand side of (1), Ω is the element area, and V_i is the unknown potential. To use the Galerkin method, the weighting functions are set the same as the base functions, and since the matrix coefficients S_{ij} are determined from the basis functions Φ_i, system (3) can be solved for the unknown node variables V_i. It should be noted that the basis function Φ_i refers to the ith node. An in-house Gaussian elimination solver was developed to solve the global system matrix.

C. The Self-Consistent Algorithm

All electron gun codes, used for designing intense beam guns, are said to be self-consistent if their solvers take into account the space-charge contribution to evaluate the static fields and the static fields forces contribution that act on the particles. The flowchart in Fig. 1 presents the successive approximation method. This procedure is repeated until the convergence criterion of the nth iteration is closer to the previous one, the $(n-1)$th. The convergence criteria may be the slopes of the particle paths or the electric field intensity in some chosen plane. However, the scheme adopted in this work takes into account the variation of the current density between two consecutive approximations. In this work, an absolute relative error of current density, between two consecutive approximations, of 0.01% was adopted. Usually, 7–16 iterations are required to reach the desired accuracy.

The calculation of the charge deposition increment $\Delta\rho_j$, at the jth triangular element of the mesh, is straightforward and is given by

$$\Delta\rho_j = \frac{q_i}{\Delta V_j} = \frac{I_i \Delta\tau}{\Delta V_j} \tag{7}$$

where I_i is the ith macroparticle current, $\Delta\tau$ is the transit time inside the jth element, and ΔV_j is the volume of the jth element. For the planar diode, using the Child–Langmuir law [8], the ith macroparticle current at the $(n+1)$th iteration $I_i^{(n+1)}$ is approximated by

$$I_i^{(n+1)} = \left(\frac{4\sqrt{2}}{9}\right) A_i \varepsilon_0 \sqrt{\eta} \left[\frac{\left(V_{j_i}^{(n)}\right)^{3/2}}{d_s^2}\right] \tag{8}$$

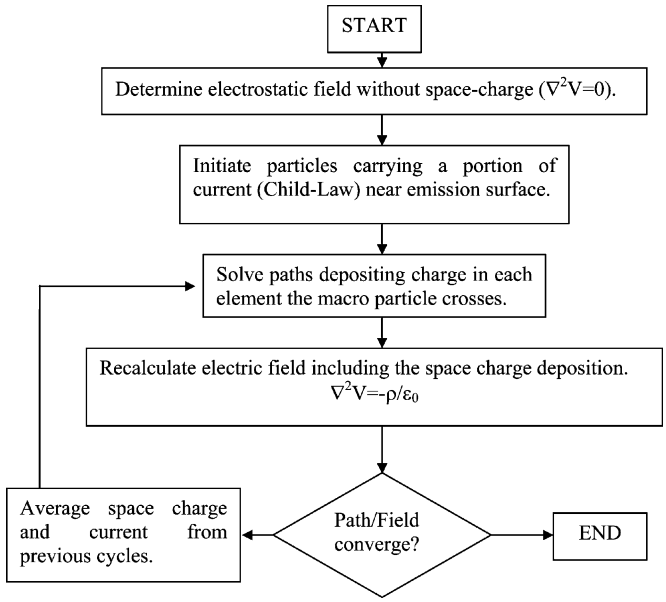

Fig. 1. Flowchart of the successive approximation method.

where A_i is the area of the cathode that contributes to the ith macroparticle, ε_0 is the vacuum permittivity, η is the particle charge-mass ratio, $V_{ii}^{(n)}$ is the jth finite element, ith particle potential evaluated at the center of the ith path located at the distance d_s, where d_s is the macroparticle distance normal to the cathode. The macroparticles start at a distance d_s from the cathode since, under the space-charge limited condition, the fields and the particle velocities at the cathode are null and they would never advance.

To avoid current density divergences, the jth element charge at the $(n+1)$th iteration ρ_j^{n+1} is averaged as

$$\rho_j^{n+1} = (1-w)\rho_j^{n-1} + w\rho_j^n \tag{9}$$

where w represents the under-relaxation factor $(0.0 \leq w \leq 1.0)$. At the first iteration, w is set to 1.0. A low value of w corresponds to the average charge density over several cycles.

Charge deposition between the cathode and the emission region follows the procedure adopted by [9]. The macroparticles move backward from the emission surface to the cathode at a constant velocity υ_b of

$$\upsilon_b = -\left(\frac{2}{3}\right)\sqrt{2\eta V_{js}} \tag{10}$$

where V_{js} is the jth particle potential at the distance d_s.

Because the initial current is too high, a suppression factor is used in the first iteration cycles. Therefore, the initial current in the first, second, and third cycles is multiplied by 0.25, 0.50, and 0.75, respectively.

III. Results

In order to validate the code, a benchmark consisting in a Pierce diode with a cathode–anode separation is of 2 cm, a cathode emission height is of 1.5 cm, and a focusing electrode height of 2.5 cm was considered. Otherwise specified, the anode voltage was set to 1 kV, the under-relaxation factor $w = 0.4$, and the number of macroparticles was set to 40.

TABLE I
MESH DATA USED TO VALIDATE THE XMGUN CODE

Mesh	Nodes	Elements	Simulation Time (sec)
I	284	499	2.8
II	486	875	3.3
III	958	1792	8.5
IV	1870	3560	22.7

System: XP with SP2, Intel Q6600 2.4 GHz with 3.0Gb RAM

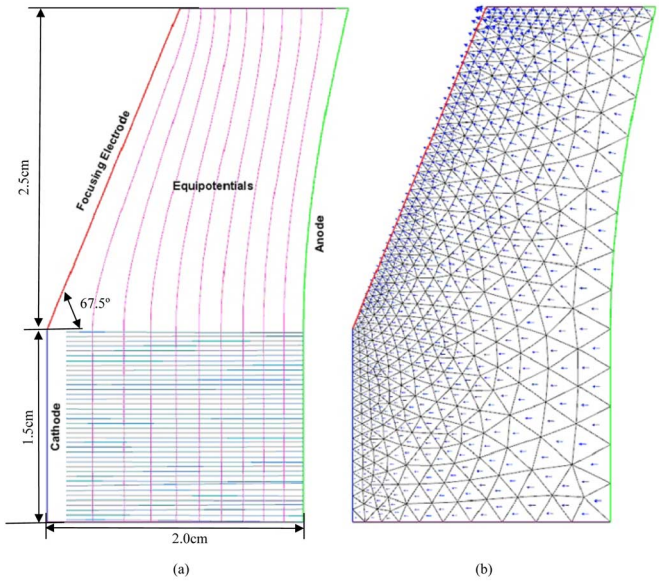

Fig. 2. For the self-consistent field solution, a detailed view of (a) 40 particle paths and the equipotentials, and (b) the mesh and the electric field.

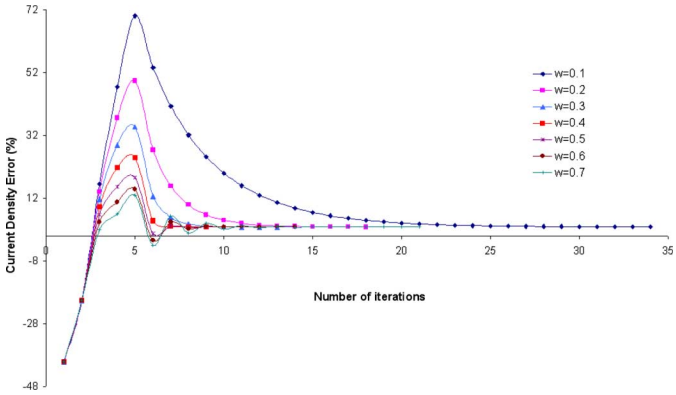

Fig. 3. Relative error of the current density J versus iteration, using various under-relaxation coefficients.

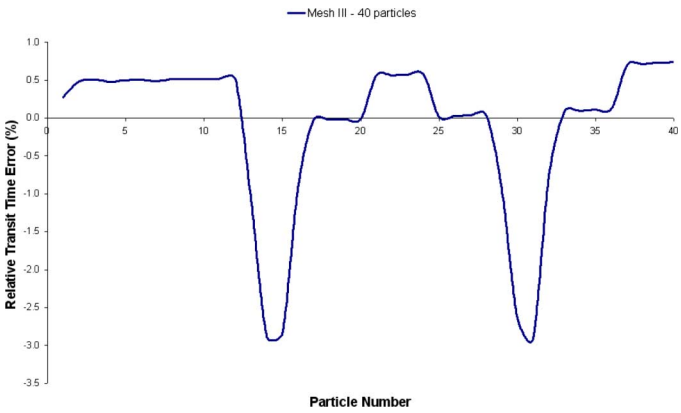

Fig. 4. Typical behavior of the relative transit time error observed during simulations.

Under space-charge limited condition, the paths must be parallel [8]. Four mesh models were analyzed according to Table I. In all the models, a refined mesh was used closer to the cathode, while a coarse one closer to the anode.

Fig. 2(a) indicates that each particle trajectory is nearly parallel. Although it is not easy to observe [Fig. 2(b)], the electric field vanishes closer to the cathode. These behaviors show good agreement with the analytical solution [8].

The current density error decreases as the mesh model is refined. Mesh I presented an error of less than 1% while that of Mesh IV was less than 0.6%. No significant improvement by increasing the number of particles was observed.

The process of convergence to the correct self-consistent fields depends on the under-relaxation coefficient w, which plays an important role since the convergence depends on it. A faster convergence rate was obtained for $0.2 \leq w \leq 0.6$.

Fig. 3 indicates that an initially higher under-relaxation factor provides minor errors. To improve the convergence rate, the use of a variable w may be adopted.

There are three quantities available to validate the quality of the beam calculation: the particle final position, the transit time, and the particle energy. With regard to the final position, it is known that the particle trajectories, in the Pierce planar diode, are parallels. Using Mesh III with 500 particles, it was found that the particles were parallel to within $\pm 0.35^{\circ}$ at the anode. During the simulations, no deviation errors exceeding $\pm 0.8^{\circ}$ at the anode were observed.

The quality of the beam, due to the transit time τ, is done knowing that, since the paths are parallel

$$\tau = \int_{d_s}^{d_a} \frac{du}{v(u)} \tag{11}$$

where $v(u)$ is the macroparticle velocity, d_a is the cathode–anode separation, and d_s is the macroparticle's starting position. Due to the energy conservation law and the scalar potential for the Pierce planar diode, the transit time is written as

$$\tau = \frac{3d_a^{2/3}}{\sqrt{2\eta V_a}} \left(d_a^{1/3} - d_s^{1/3} \right). \tag{12}$$

Typically, transit time errors below 4% were observed. Fig. 4 depicts a usual output obtained during simulations.

To validate the particle energy, it was observed whether the particles conserve their energy as they travel from the cathode to the anode. Four planes were used to measure the particle energies. The planes were located at 10.9%, 40.6%, 80.2%, and 98.2%, along the space separating the cathode and the anode. Planes closer to the emission area had higher errors. Regarding the plane located at 10.9%, which presented the worst result, it

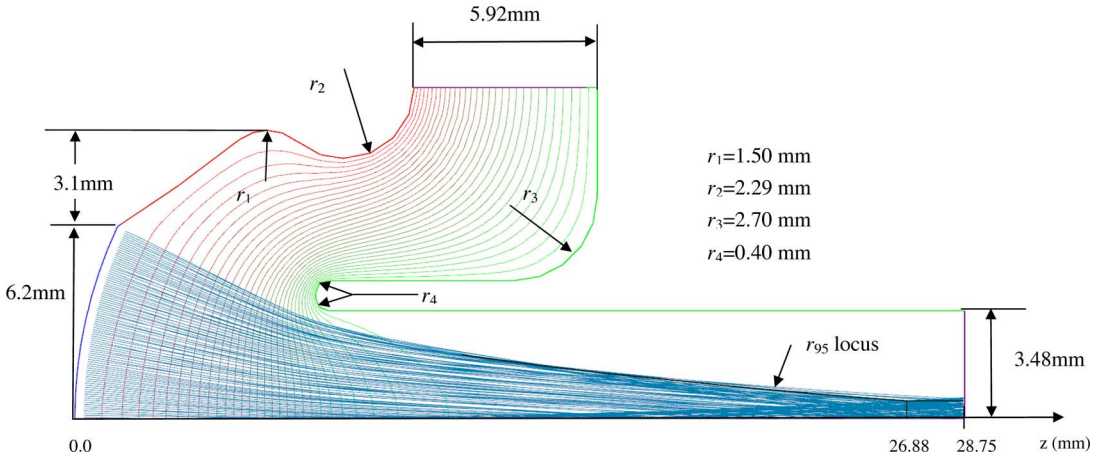

Fig. 5. Electron gun simulation using the particles path equations approach.

was observed that the use of Mesh I produced relative energy errors not greater than 3%, while using Mesh IV produced relative energy errors below 0.4%. Therefore, refined meshes led to a better particle energy response.

A gun model for use in a typical power microwave tube (Fig. 5) was also simulated.

The gun was modeled using cylindrical symmetry, 90 macroparticles, with cathode curvature and cathode-disc radii of 14.59 and 6.2 mm, respectively, and 30 kV at the anode. The gun's mesh contained 2796 nodes and 5057 elements. Eight iterations were needed to reach a current density difference below 0.1% between two consecutive cycles using $w = 0.3$. This gun yields a current of 7.10 A and a perveance of 1.37 μPerv. A current of 7.54 A and a perveance of 1.45 μPerv were observed running an EGUN simulation for the same gun model. The 1-kV equipotentials are also shown in Fig. 5.

A figure of merit used as reference in measuring the quality of the electron beam is [10] the normalized transverse velocity σ

$$\sigma = \left\{ \left[\sum_{i=1}^{n} I_i (\alpha_i - \langle \alpha \rangle)^2 \right] / I_0 \right\}^{1/2} \tag{13}$$

where α_i is the slope of the ith macroparticle path as it crosses a given plane, I_i is the current transported by the ith macroparticle path, I_0 is the total current crossing the plane, and $\langle \alpha \rangle$ is the weighted mean macroparticle path slope of the n macroparticles that cross a given plane perpendicular to the z-axis, given by

$$\langle \alpha \rangle = \left(\sum_{i=1}^{n} I_i \alpha_i \right) / I_0. \tag{14}$$

The lower the value of σ is, the better is the laminarity of the beam under analysis. The minimum beam radius containing 95% of the current, r_{95}, was found in position $z = 26.88$ mm. In this position, it was observed that $\langle \alpha \rangle = -2.7\pi$ mrad and $\sigma = 0.068$.

IV. Conclusion

A FEM formulation to solve the coupled Poisson equation for the scalar potential and the nonlinear second-order differential equation for the nonrelativistic electrons path were described. A Pierce planar diode benchmark indicated current density errors below 1%. The under-relaxation factor w plays an important role in the number of iterations, since it may establish faster convergence solutions. To validate the quality of the beam, such as the macroparticle deviation, transit time, and energy, benchmarks were performed and good agreement with the theoretical results was demonstrated. The use of the particle path approach led directly to the macroparticles minimum of the path that would be used to estimate the beam waist and beam waist distance from the cathode.

Acknowledgment

The authors would like to thank Dr. A. Laudani for his invaluable suggestions that improved the results, Prof. W. B. Herrmannsfeldt for his assistance with the EGUN, and Prof. S. Humphries for his willingness to clarify some doubts regarding the charge deposition scheme adopted by TRACK. This work was supported by FINEP (Research and Projects Financing) under Contract 01.09.0049.00.

References

[1] W. B. Herrmannsfeldt, Stanford Linear Acc. Center SLAC-331, 1988, unpublished.
[2] S. Humphries, Jr., "TRACK," in *Computational Accelerator Physics*, R. Ryne, Ed. New York: AIP, 1994, p. 597.
[3] J. E. Petillo *et al.*, "The MICHELLE electron gun and collector modeling tool: Theory and design," *IEEE Trans. Plasma Sci.*, vol. 30, pp. 1238–1264, Jun. 2002.
[4] S. Coco *et al.*, "3-D finite-element analysis of TWT grid electron guns," *IEEE Trans. Magn.*, vol. 43, no. 4, pp. 1233–1236, Apr. 2007.
[5] P. Girdinio, M. Repetto, and J. Simkin, "Finite element modelling of charged beams," *IEEE Trans. Magn.*, vol. 30, no. 5, pp. 2932–2935, Sep. 2004.
[6] J. P. A. Bastos and N. Sadowski, *Electromagnetic Modeling by Finite Element Methods*. New York: Routledge, 2003.
[7] P. P. Silvester and R. L. Ferrari, *Finite Elements for Electrical Engineers*, 3rd ed. Cambridge, U.K.: Cambridge Univ. Press, 1996.
[8] J. R. Pierce, *Theory and Design of Electron Beams*. Princeton, NJ: Van Nostrand, 1949.
[9] S. Humphries, Jr., *Field Solutions on Computers*. Boca Raton, FL: CRC Press, 1997, Section 10.7.
[10] R. True, "A theory for coupling gridded gun design with PPM focusing," *IEEE Trans. Electron Devices*, vol. ED-31, no. 3, pp. 353–362, Mar. 1984.